Title

A Framework for Global Multicategory and Multiscalar Drought Characterization Accounting for Snow Processes.

Journal

Water Resources Research, 55(11)

ISSN

0043-1397

Authors

Zhang, Baoqing
Xia, Youlong
Huning, Laurie
et al.

Publication Date

2019-11-01

DOI

10.1029/2019WR025529

Peer reviewed

Water Resources Research

RESEARCH ARTICLE
10.1029/2019WR025529

A Framework for Global Multicategory and Multiscalar Drought Characterization Accounting for Snow Processes

Baoqing Zhang[1,2], Youlong Xia[3], Laurie S. Huning[4], Jiahua Wei[2], Guangqian Wang[2], and Amir AghaKouchak[4,5]

[1]Key Laboratory of Western China's Environmental Systems (Ministry of Education)College of Earth and Environmental Sciences, Lanzhou University, Lanzhou, China, [2]State Key Laboratory of Hydroscience and EngineeringDepartment of Hydraulic Engineering, Tsinghua University, Beijing, China, [3]I. M. Systems Group at Environmental Modeling Center, National Centers for Environmental Prediction, College Park, MD, USA, [4]Department of Civil and Environmental Engineering, University of California, Irvine, CA, USA, [5]Department of Earth System Science, University of California, Irvine, CA, USA

Key Points:
- A global multi-scalar drought index (SZI_{snow}) was developed to improve the drought characterization by incorporating snow processes
- The SZI_{snow} generally performs better than the SZI for monitoring multi-category droughts by considering snow dynamics
- The SZI_{snow} incorporates water-energy budgets to address the influence of snow on both the water supply and demand in drought assessment

Supporting Information:
- Supporting Information S1

Correspondence to:
J. Wei and G. Wang,
weijiahua@tsinghua.edu.cn;
dhhwgq@tsinghua.edu.cn

Citation:
Zhang, B., Xia, Y., Huning, L. S., Wei, J., Wang, G., & AghaKouchak, A. (2019). A framework for global multicategory and multiscalar drought characterization accounting for snow processes. *Water Resources Research*, *55*, 9258–9278. https://doi.org/10.1029/2019WR025529

Received 9 MAY 2019
Accepted 26 SEP 2019
Accepted article online 10 OCT 2019
Published online 19 NOV 2019

Abstract Drought indices do not always provide the most relevant information for water resources management as most of them neglect the role of snow in the land surface water balance. In this study, a physically based drought index, the Standardized Moisture Anomaly Index (SZI), was modified and improved by incorporating the effects of snow dynamics for drought characterization at multiple time scales. The new version of the SZI, called SZI_{snow}, includes snow in both the water supply and demand in drought characterization by using the water-energy budgets from the Global Land Data Assimilation Systems product. We compared and evaluated the performance of SZI_{snow} and SZI in drought identification globally across various time scales using observed multicategory drought evidences from several sources. Results show that the SZI_{snow} agrees better with the observed changes in hydrological and agricultural droughts than the SZI, particularly over basins with high snow accumulation. Furthermore, the SZI_{snow} is more consistent with the residual water-energy ratio than the SZI over snow-influenced regions. Overall, the SZI_{snow} can be either a complement or an improvement over the SZI for identifying, monitoring, and characterizing hydrological and agricultural droughts at various scales (e.g., 1–48 months) over high-latitude and high-elevation regions that receive snow.

1. Introduction

Determining the occurrence and evolution of drought at various temporal scales is a challenging task due to the lack of long-term measurements of surface water-energy fluxes and states, including streamflow, radiation, evapotranspiration (*ET*), soil moisture, and snow water equivalent (SWE) (Stagge, Kohn, et al., 2015, 2017). Unlike other natural disasters (e.g., hurricanes, rainstorms, and floods), the complexity of quantifying a drought arises from the lack of a specific physical variable that can directly represent its onset, ending, and severity (AghaKouchak et al., 2015; Yang, Roderick, et al., 2018). Moreover, the definition of drought often varies with application and research interests (e.g., meteorological, hydrological, and agricultural droughts), which further contributes to difficulties associated with drought quantification (McEvoy et al., 2012; Yang, Zhang, et al., 2018; Zhang et al., 2019). A precipitation deficiency is primarily referred to as meteorological drought; a hydrological drought is commonly caused by a deficit in streamflow or low surface and groundwater levels; and an agricultural drought mainly results from low levels of soil moisture storage. Moreover, drought can occur across a variety of temporal scales (e.g., 1–48 months), which is a critical consideration for monitoring droughts, as knowledge of its multiscalar nature facilitates the quantification of the lag among meteorological, hydrological, and agricultural droughts (McKee et al., 1993; Vicente-Serrano, Beguería, et al., 2012; Zhang et al., 2015).

Increased temperatures and atmospheric evaporative demand (Wang et al., 2012; Yin et al., 2014) is expected to reduce the amount of snowfall and SWE (Barnett et al., 2005; Margulis et al., 2016) resulting in more frequent or intense droughts (Arheimer et al., 2017; Huning & AghaKouchak, 2018; Jones & Moberg, 2003). Several studies have shown that warming processes, resulting in increased *ET* and/or soil moisture

deficits, markedly affect the severity of droughts (Dai, 2011, 2013; Sheffield et al., 2012; Sheffield & Wood, 2008; van der Schrier et al., 2011; Vicente-Serrano et al., 2010; Vicente-Serrano et al., 2014; Zhang et al., 2017). In addition, as the atmosphere warms and less precipitation (P) falls as snow, the snow-covered region (period) becomes smaller (shorter), and snowmelt occurs earlier in spring, leading to a shift in peak runoff that may increase the time lag between the peak in water availability and demand in many regions (Barnett et al., 2005). A prolonged imbalance of surface water and moisture deficiencies caused by the changing snowpack could results in more frequent hydrological and agricultural droughts, further threatening water security (Trenberth et al., 2014). Therefore, the effects of snow dynamics on water availability from global warming warrant further investigation (Jenicek et al., 2016) since snow directly affect the onset, duration, severity, and spatial extent of droughts (Staudinger et al., 2014), even without a change in P. Thus, considering the importance and complexity of snow in drought evolution, it is necessary to incorporate snow information into global drought monitoring.

A number of efforts have been undertaken to develop methods for drought characterization (e.g., Palmer, 1965; McKee et al., 1993; Wells et al., 2004; Sheffield & Wood, 2007; Vicente-Serrano et al., 2010; Hao & AghaKouchak, 2013; Mu et al., 2013; Zhang et al., 2014, 2015, 2017); however, they generally neglect the effects of snow dynamics on drought evolution (Staudinger et al., 2014). Among them, drought indices are commonly used to identify drought occurrences, and thus, developing such an index for various applications is essential to drought monitoring and prediction (Zhang et al., 2015). The majority of drought monitoring studies have been conducted using either (1) the Palmer drought index, including Palmer Drought Severity Index (PDSI; Palmer, 1965) and self-calibrated PDSI (Wells et al., 2004) or (2) a standardized index, including standardized precipitation index (McKee et al., 1993) and standardized precipitation evapotranspiration index (SPEI; Vicente-Serrano et al., 2010), which do not incorporate the snow information needed for more robust assessments of drought in snow-dominated regions.

The PDSI was created to measure the cumulative departure (relative to local mean conditions) of the surface moisture supply and demand (Mishra & Singh, 2010) by incorporating antecedent P, runoff, ET, and changes in soil moisture storage. However, it lacks the ability to identify drought events at multiple time scales (Wells et al., 2004; Vicente-Serrano et al., 2010, Vicente-Serrano, Beguería, et al., 2012; Zhang et al., 2015). Although the SPEI (Vicente-Serrano et al., 2010) can be used to identify droughts at various time scales (Beguería et al., 2014), its main drawback relates to uncertainties in estimating potential evapotranspiration (PET) as a proxy for the overall water demand (Sheffield et al., 2012; Trenberth et al., 2014; Yang et al., 2006, 2007; Zhang et al., 2015).

More recently, the Standardized Moisture Anomaly Index (SZI; Zhang et al., 2015) was developed to capture the onset, ending, and severity of a multiyear drought event at a variety of time scales using water budget simulations produced with a physically based land surface model (LSM). The SZI leverages one of the strengths of the PDSI by using the moisture anomaly index (Z) as indicator of surface water deficiency or surplus. Zhang et al. (2015) demonstrated that the variability of the SZI is more consistent with observed drought evidences than that of the SPEI over water-stressed regions because the SZI provides a more reasonable estimation of the water demand (or the climatically appropriate for existing conditions P, defined as $\widehat{P}$) by including of ET, runoff, and changes in soil moisture storage (Zhang et al., 2015). By combining the water demand estimates ($\widehat{P}$) from the PDSI and the multiscalar nature of the SPEI, the SZI overcomes many weaknesses associated with the PDSI and SPEI. The shortcomings of the SZI are: (1) the need for information about many surface water-energy components as input data (often more than many other drought indices); (2) the use of a sophisticated LSM to estimate these hydrological inputs, which can be time consuming; (3) the negligence of the effects of snow in drought characterization. In addition, it should be noted that both SPEI and SZI rely on the selection of a univariate probability distribution to standardize the indices, allowing for comparisons across climate zones (Stagge, Tallaksen, et al., 2015, 2016; Zhang et al., 2015). The choice of a probability distribution to standardize the SPEI and SZI may impart different results for the computed drought indices (Stagge, Tallaksen, et al., 2015, 2016).

The above described limitations of current drought indices highlight the need to incorporate snow information into a drought index such as the SZI to better characterize, model, and forecast droughts worldwide. Staudinger et al. (2014) proposed the Standardized Snow Melt and Rain Index, which accounts for rain and snowmelt deficits that effectively influence streamflow droughts. Although the Standardized Snow

Melt and Rain Index is derived using temperature and precipitation to model snow instead of directly incorporating snow data, it provides some insights on how to upgrade the SZI for drought identification in snow-dominated regions (Staudinger et al., 2014). To date, some analyses have been performed with this in mind by considering the effects of snowfall/snow on drought assessment (Margulis et al., 2016; Potopová et al., 2016; van der Schrier et al., 2013; Yan et al., 2014, 2016). However, the aforementioned studies were focused on the water supply instead of more broadly understanding the effect of snow on both the water supply and demand in drought quantification.

The main objective of this study is to (1) improve the SZI by incorporating snow information in both the water supply and demand using the Global Land Data Assimilation System (GLDAS; Rodell et al., 2004; i.e., establish the SZI with snow, SZI_{snow}) and (2) evaluate the performance of the resulting SZI_{snow} by comparing it with SZI and observed drought evidences from multiple sources. The conceptual and technical improvement of the SZI_{snow} compared to the SZI is the key point of this work. This study contributes to the further development of drought indices by demonstrating how incorporating snow processes can improve the physical realism of drought assessment, especially in high-latitude and high-elevation regions covered by a deep snowpack. This work evaluates the snow states (e.g., SWE, snow depth [SNWD]) from the GLDAS product relative to observations. This study also examines different types of water-energy responses to water deficits across a variety of regions, with particular emphasis on snow-covered regions.

2. Data and Methods

2.1. Data Sets

2.1.1. Snow Observations

The observed daily SWE and SNWD data for the western United States (includes 712 observation sites) and Alaska, United States (includes 31 observation sites) from October 1978 to September 2013 were obtained from the Snowpack Telemetry network operated by the Natural Resources Conversation Service (http://www.wcc.nrcs.usda.gov/nwcc/inventory). The observed monthly SNWD data for the Xinjiang region of China (includes 105 observation sites) from 1961–2013 were obtained from the Xinjiang Meteorological Bureau. The observed monthly SNWD and SWE data in eastern China (includes 110 observation sites) over 1980–2009 were provided by the National Meteorological Information Center of China (http://data.cma.cn/site/index.html; Wang et al., 2016). All SNWD and SWE observations were used to evaluate the performance of the snow variables from the GLDAS products.

2.1.2. GLDAS Products

The GLDAS was developed by integrating ground-based and satellite-based observations to drive four offline LSMs (Chen et al., 2013; Rodell et al., 2004; Wang et al., 2011). Using land surface modeling and data assimilation, the widely used GLDAS provides optimal values of land surface fluxes and states for hydrometeorology studies, particularly at regional scales or over areas with limited observations. Since the GLDAS provides sufficient water-energy variables for calculating the SZI at global scales and users do not need to run LSMs themselves, directly using GLDAS to compute the SZI could overcome the first and the second shortcomings of the SZI methods described above. Since the GLDAS product provides snowfall, SWE and snowmelt runoff at the global scale, these fields can be incorporated into the SZI.

Currently, there are two versions of the GLDAS product: GLDAS-1 and GLDAS-2. The GLDAS-1 drives four LSMs at a spatial resolution of $1° \times 1°$ from 1979 to 2017, including the Community Land Model (CLM; Dai et al., 2003), the Mosaic model (Koster & Suarez, 1994), the Noah model (Chen et al., 1996; Koren et al., 1999), and the Variable Infiltration Capacity (VIC) model (Liang et al., 1994). The GLDAS-2 only drives the Noah model at a spatial resolution of $0.25° \times 0.25°$ from 1948 to 2010. Both GLDAS-1 and GLDAS-2 data sets are available via Goddard Earth Sciences Data and Information Services Center (http://disc.sci.gsfc.nasa.gov/hydrology/data-holdings). Since the GLDAS-2 Noah LSM product performs best in its simulation of the land water-energy states and fluxes in most regions of the global land area (details in the supporting information Figures S1–S6), we use its monthly land surface variables to calculate the SZI and SZI_{snow} in this work.

In addition, the ability of GLDAS-2 Noah LSM to accurately reproduce snow processes is an important cornerstone in the development of our drought index. To verify the reliability of its inputs for use in the SZI and

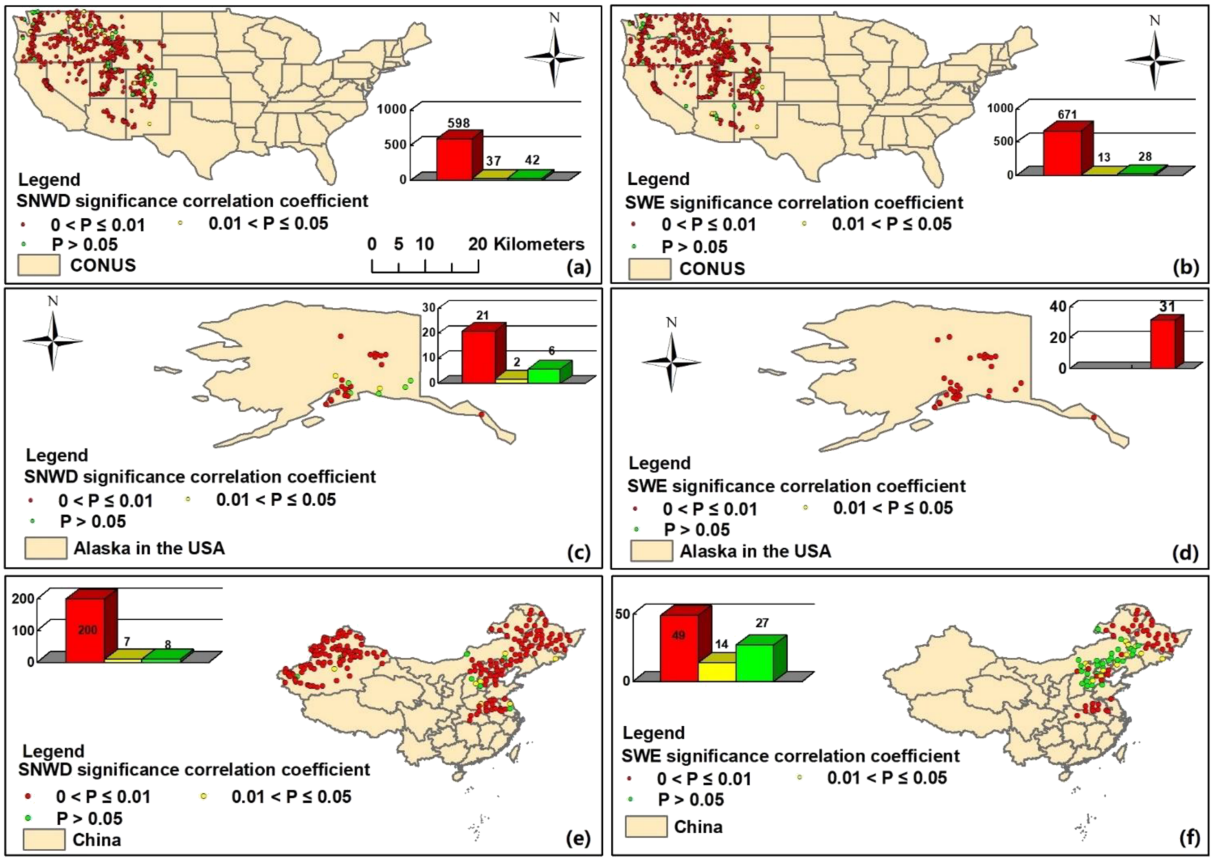

Figure 1. Evaluation of snowpack data simulated by the GLDAS-2 Noah LSM using observations in the western United States (a, b), Alaska (c, d), and China (e, f). SNWD = snow depth; SWE = snow water equivalent.

SZI_{snow}, SWE and SNWD from the GLDAS-2 Noah LSM (hereafter, GLDAS-2 refers to the GLDAS-2 Noah LSM product) are evaluated against in situ snow observations from 958 stations over three regions (i.e., western United States, Alaska, and China). Figure 1 summarizes the statistical significance of the correlations between observed and GLDAS-2 monthly SNWD and SWE. In the western United States, statistically significant correlations ($p < 0.05$) were found between observations of SNWD and SWE and those from GLDAS-2 at 635 stations (94% of the total number of stations; Figure 1(a)) and 684 stations (~96% of the total stations; Figure 1(b)). The GLDAS-2 SNWD and SWE over Alaska also show significant correlations with the observations at most stations (Figures 1(c) and 1(d)). Correlating monthly SNWD and SWE from GLDAS-2 with observations in China (Figures 1(e) and 1(f)) indicated that statistically significant correlations exist for the SNWD case at 207 stations (96% of all 215 stations), whereas only 63 stations (or 70% of the 90 stations) exhibit significant correlations when GLDAS-2 SWE was correlated with the observations. This likely results from biases in the meteorological forcing such as *P*, air temperature, rain-snow partitioning, as well as model structure (e.g., single snow layer model), and parameter assumptions. In general, this demonstrates that the GLDAS-2 reasonably represents the observed SNWD and SWE variability and serves as a viable data set for providing snow and land surface state/flux information. Nonetheless, detailed analysis explaining the underperformance of GLDAS-2 (relative to observations) in some parts of northeastern China is provided in section 4.

The surface meteorological forcing (e.g., *P*, 2-m air temperature), model-simulated *ET*, and runoff/streamflow are also validated against either the observations or satellite-based products (see Figures S1–S6). Overall, the GLDAS-2 forcing and Noah-simulated surface water-energy budgets have better performance (larger correlations and smaller normalized root mean square error values) when compared with GLDAS-1 and four LSMs simulations, suggesting a good alternative. Given the relative complexity of the LSM used to generate all hydrometeorological variables, the simulated variables could potentially introduce biases into the SZI and

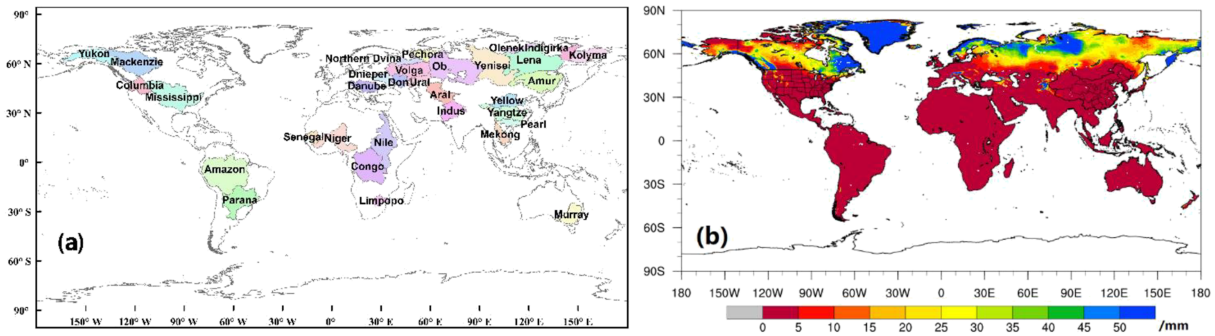

Figure 2. Locations of 32 large study basins a and global distribution of long-term annual mean snow water equivalent b.

SZI_{snow} when comparing different sites/grids. We assume that overall effects on large basins investigated in this study are small.

2.1.3. Drought Evidence Used for Evaluating the Performance

The monthly Climatic Research Unit time series Version 4.01 (CRU TS 4.01 gridded data, with a 0.5° × 0.5° resolution; http://www.cru.uea.ac.uk/cru/data/hrg/) climate data (Harris et al., 2014) and global daily *ET* product (Global Land Evaporation Amsterdam Model (GLEAM) v3.1a, at a spatial resolution of 0.25° × 0.25°; https://www.gleam.eu/) from 1980 to 2010 (Martens et al., 2017; Miralles et al., 2011) were used to determine the residual water-energy ratio (WER; $WER = (P - ET)/(PET - ET)$) in drought conditions (for a detailed description of *WER*, see section 2.2.4; Liu et al. (2017)), wherein *PET* is calculated with the Penman-Monteith equation (Allen et al., 1998). The observed monthly terrestrial water budget data set (including streamflow and soil water storage data) for 32 large study basins (Figure 2(a)) over the period of 1984–2006 was used to evaluate the performance of SZI and SZI_{snow} across the globe (Pan et al., 2012). Pan et al. (2012), Xu et al. (2013), and Liu et al. (2017) developed this data set using multiple observation sources (including basin-averaged streamflow data). Basin area, location, and long-term annual mean hydrometeorological states and fluxes of the 32 large global basins (i.e., basin area and location and long-term annual mean hydrometeorological states and fluxes) are provided in Figure 1 and Table 1.

2.2. Methodology

2.2.1. Hydrological Accounting

Four monthly water budget components and their potential values were retrieved from the LSM simulations to estimate the regional water demand and carry out the hydrological accounting. These variables are runoff (*RO*), potential runoff (*PRO*), *ET*, *PET*, soil infiltration (*R*), potential soil infiltration (*PR*), soil moisture loss (*L*), and potential soil moisture loss (*PL*) as depicted in Figure 3(a). Soil moisture storage is regarded as a water reservoir in the SZI. Any changes in soil moisture storage (loss or infiltration) would influence the surface water balance (i.e., supply of water or demand of water). Contrary to the SZI, which systematically neglects snowfall as a water source and the impact of snow on surface hydrological processes (Figure 3(a)), the snow processes are introduced as another water reservoir in the water budget for SZI_{snow} (Figure 3(b)). Besides the soil moisture storage, snowpack changes (melt or accumulation) would also affect the surface water balance (i.e., supply of water or demand of water) and the drought condition quantified by SZI_{snow}. As a result, the physical processes incorporated in the SZI_{snow} are more comprehensive than those in the SZI, making it applicable to a broader set of climatic regions and thereby, a broader, global community. Additionally, SZI_{snow} also accounts for the total amount of rainfall and snowfall (Figure 3(b)).

In addition to the above four water budget components and their potential values used in the hydrological accounting of SZI, two snowpack variables (snowmelt [*SM*] and SWE accumulation [*SA*]) and their potential values (potential snowmelt [*PSM*] and potential SWE accumulation [*PSA*]) are taken into account in the SZI_{snow} estimation of the total water demand (Figure 3(b)). The variables used to compute the SZI_{snow} are given by:

Table 1
Physical Characteristics and Long-Term Annual Hydrologic States and Fluxes for 32 Large Basins Used to Evaluate the SZI_{snow}

River basin	Drainage area (10^4 km^2)	Cumulative P (mm)	Mean SWE (mm)	Mean SNWD (mm)	Tair (°C)	SurfT (°C)
Pechora	32	525.6	47.5	268.2	−3.0	−3.5
Northern Dvina	36	598.2	37.6	196.8	1.2	0.5
Yenisei	256	443.2	31.9	229.4	−5.7	−5.4
Kolyma	64	266.0	30.2	276.8	−12.9	−12.8
Olenek	21	268.2	29.2	272.4	−13.6	−13.4
Volga	139	552.1	25.3	140.0	3.9	3.4
Ob	299	429.3	24.0	164.4	0.1	0.1
Columbia	67	594.2	23.9	94.3	6.2	6.4
Mackenzie	175	358.4	23.3	180.0	−4.3	−4.1
Lena	243	354.1	23.1	218.0	−10.0	−9.4
Indigirka	34	238.2	16.9	204.8	−16.9	−16.3
Yukon	83	244.1	14.3	103.0	−6.2	−5.7
Aral	123	246.6	9.8	52.5	9.3	10.5
Ural	24	280.6	9.0	68.5	5.5	6.2
Don	43	450.6	8.6	50.2	7.5	7.7
Dnieper	50	564.0	7.8	40.3	7.4	7.3
Danube	82	751.1	7.7	31.3	9.0	9.0
Amur	186	503.2	5.6	55.3	−1.2	−0.4
Indus	114	375.1	3.7	21.9	16.1	17.5
Mississippi	320	729.8	1.5	10.7	10.3	10.8
Yangtze	180	986.2	0.2	1.1	11.3	11.9
Yellow	80	385.6	0.2	1.1	6.9	8.2
Mekong	81	1447.1	0.1	0.4	21.3	22.0
Murray-Darling	106	440.9	0.0	0.2	17.6	19.2
Pearl	45	1417.3	0.0	0.1	19.1	19.5
Amazon	692	2117.1	0.0	0.0	25.0	25.5
Parana	264	1170.4	0.0	0.0	21.9	22.6
Limpopo	42	520.2	0.0	0.0	21.1	22.6
Nile	308	594.9	0.0	0.0	25.5	27.6
Niger	212	648.8	0.0	0.0	27.6	29.2
Senegal	44	509.2	0.0	0.0	28.7	30.5
Congo	370	1459.5	0.0	0.0	23.9	25.0

Note. Tair = annual mean air temperature; SurfT = annual mean surface skin temperature; and SNWD = snow depth.

$$\begin{cases} RO = RO_s + RO_b + RO_{sm} \\ PRO = AWC - PR \end{cases} \tag{1}$$

where RO_s, RO_b, and RO_{sm} are the surface runoff, baseflow-groundwater runoff, and snowmelt runoff, respectively; AWC is the available soil water holding capacity of the two layers, which is estimated as the maximum value of soil moisture over each grid cell. ET and PET are given by:

$$\begin{cases} ET = E_b + E_t + E_i \\ PET \text{ is calculated using Penman-Monteith equation} \end{cases} \tag{2}$$

where E_b, E_t, and E_i are the bare soil evaporation, transpiration, and canopy water evaporation, respectively. The RO_s, RO_b, RO_{sm}, E_b, E_t, and E_c are directly obtained from GLDAS-2.

The soil profile is divided into two layers (Figure 3(b)), where the surface layer and underlying soil layer extend from 0–100 mm and 100–2,000 mm, respectively. The soil infiltration and potential infiltration are calculated as follows:

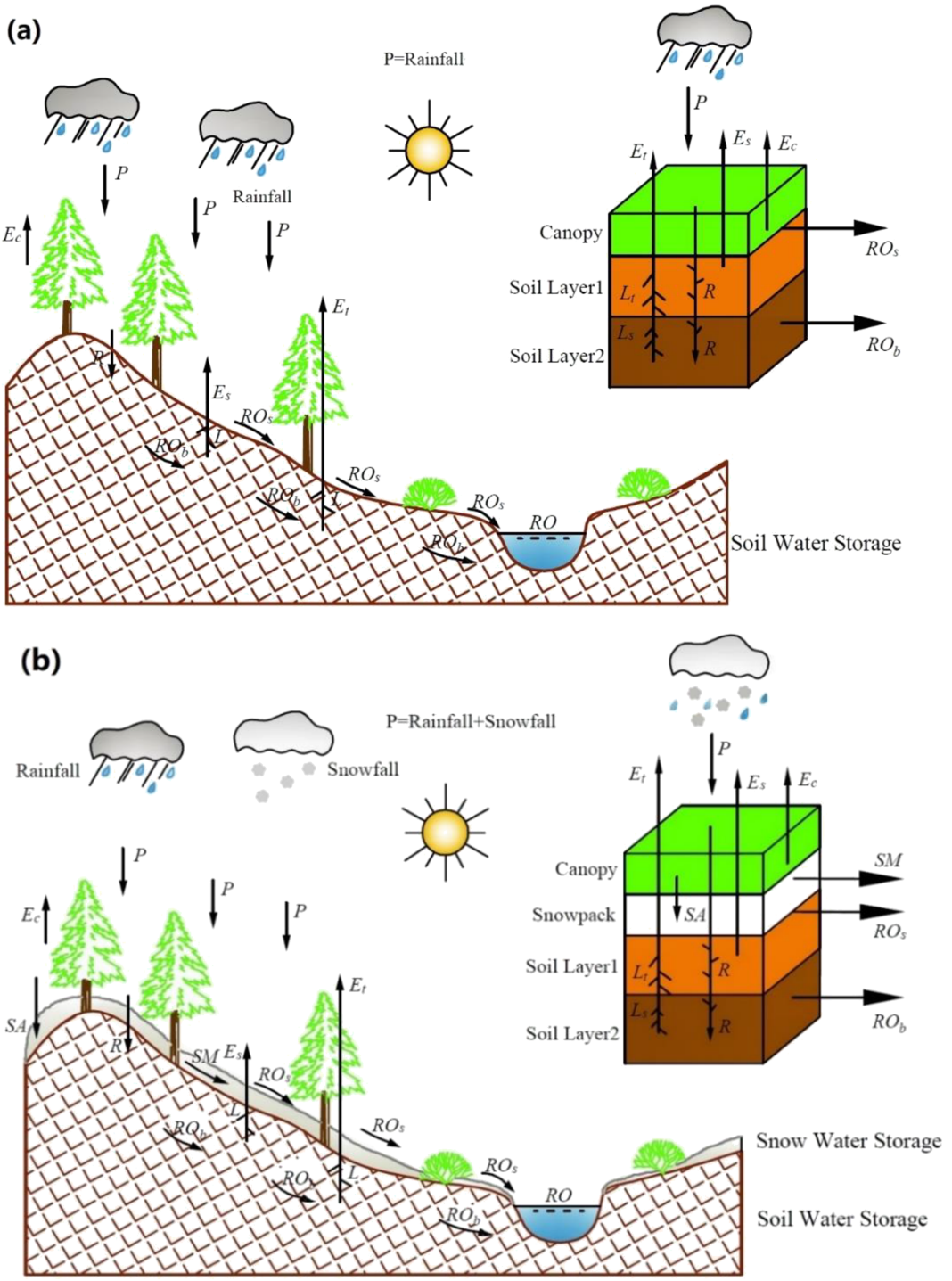

Figure 3. Schematic of the physical mechanisms included in the SZI (a) and SZI_{snow} (b; see section 2.2.1 for descriptions of variables). SZI = standardized moisture anomaly index.

$$\begin{cases} R = \begin{cases} \Delta S_t + \Delta S_u & \Delta S_t + \Delta S_u \geq 0 \\ 0 & \Delta S_t + \Delta S_u < 0 \end{cases} \\ PR = AWC - (S_t + S_u) \end{cases} \tag{3}$$

where the surface layer and underlying layer available soil moisture (S_t and S_u, respectively) are computed

from GLDAS-2, which in turn are used to derive their monthly changes (i.e., ΔS_t and ΔS_u, respectively). The soil moisture and potential soil moisture are given by:

$$\begin{cases} L = \begin{cases} 0 & \Delta S_t + \Delta S_u \geq 0 \\ -(\Delta S_t + \Delta S_u) & \Delta S_t + \Delta S_u < 0 \end{cases} \\ \begin{cases} PL_t = Min\ (PET,\ \ S_t) \\ PL_s = (PET - PL_t)\dfrac{S_u}{AWC} \\ PL = PL_t + PL_s \end{cases} \end{cases} \tag{4}$$

where L_t and L_s are the moisture losses from the surface and underlying soil layers, respectively. PL_t and PL_s are the potential moisture losses from the surface and underlying layers. The SWE accumulation and snowmelt and their potential values are:

$$\begin{cases} SA = \begin{cases} 0 & \Delta SWE < 0 \\ \Delta SWE & \Delta SWE \geq 0 \end{cases} \\ PSA = P_{snow} \end{cases} \tag{5}$$

$$\begin{cases} SM = \begin{cases} -\Delta SWE & \Delta SWE < 0 \\ 0 & \Delta SWE \geq 0 \end{cases} \\ PSM = SWE \end{cases} \tag{6}$$

Lastly, P_{snow} and SWE are the snowfall amount and monthly change in SWE, which are derived from the GLDAS-2 outputs. All water budget components used in this study are given in millimeter.

2.2.2. Climatic Coefficients and the Climatically Appropriate for Existing Conditions P ($\widehat{P}$)

The $\widehat{P}$ in SZI needs four water budget terms, whereas six water budget components (including SWE and snowmelt) are required for defining the water demand, $\widehat{P}_{snow}$, for the SZI_{snow}. The monthly climatic coefficients were computed as the ratios of the monthly climatic averages of the actual to potential values for ET (α_j), soil infiltration (β_j), runoff (γ_j), soil moisture loss (δ_j), snowpack accumulation (ε_j), and snowmelt (φ_j) as follows:

$$\begin{cases} \alpha_j = \overline{ET_j}/\overline{PET_j} \\ \beta_j = \overline{R_j}/\overline{PR_j} \\ \gamma_j = \overline{RO_j}/\overline{PRO_j} \\ \delta_j = \overline{L_j}/\overline{PL_j} \\ \varepsilon_j = \overline{SA_j}/\overline{PSA_j} \\ \varphi_j = \overline{SM_j}/\overline{PSM_j} \end{cases} \tag{7}$$

where j represents the month of the year (i.e., $j = 1, \ldots, 12$). These ratios are taken as weighting factors or the water balance coefficients used to compute $\widehat{P}_{snow}$ as:

$$P_{snow} = \alpha_j PET + \beta_j PR + \gamma_j PRO + \varepsilon_j PSA - \delta_j PL - \varphi_j PSM \tag{8}$$

2.2.3. Standardizing the Moisture Anomaly Series

The difference between the actual precipitation (P) and $\widehat{P}_{snow}$ is used to define the moisture anomaly Z_{snow}:

$$\begin{cases} P = P_{rain} + P_{snow} \\ Z_{snow} = P - \widehat{P}_{snow} \end{cases} \tag{9}$$

which represents the regional water deficit/surplus. Recall that in the case of SZI_{snow}, P is equal to the sum of the total amount of rainfall (P_{rain}) and snowfall (P_{snow}; i.e., $P = P_{rain} + P_{snow}$), while the P in SZI only includes rainfall. Because the SM, PSM, SA, and PSA are calculated based on SWE, the SWE has a large influence on the value of Z_{snow} and thus SZI_{snow} in snowy regions.

The computed Z_{snow} values were aggregated to different time scales (i.e., 1–48 months), following the same procedure as described for the SZI by Zhang et al. (2015). We tested four three-parameter distributions to

Table 2
Standardized Threshold Values for Drought and Wetness Classifications of SZI_{snow}, SZI, SSI, SWSI, and SWI

Value α for SZI_{snow}, SZI, SSI, SWSI, and SWI	Drought and wetness classification
Drought classification	
$\alpha < -2.0$	Extreme drought
$-2.0 \le \alpha < -1.5$	Severe drought
$-1.5 \le \alpha < -1.0$	Moderate drought
$-1.0 \le \alpha < -0.5$	Mild drought
$-0.5 \le \alpha < 0.5$	Normal
Wetness classification	
$0.5 \le \alpha < 1.0$	Mild wetness
$1.0 \le \alpha < 1.5$	Moderate wetness
$1.5 \le \alpha < 2.0$	Severe wetness
$\alpha \ge 2.0$	Extreme wetness

Note. SZI =; SSI =; SWSI =;SWI = .

model the P, D, WER, Z, and Z_{snow} values at different climate zones, including Pearson III, log logistic, lognormal, and general extreme values. Herein, we adopted a log-logistic distribution for standardizing the Z and Z_{snow} time series to obtain the SZI and SZI_{snow} in term of what the best fit was exhibited across different climate zones. This follows the approach used in Vicente-Serrano et al. (2010) and Zhang et al. (2015) for standardizing the values at each temporal scale. In the SZI_{snow}, the average value of each standardized Z_{snow} series is zero. Negative (positive) values of SZI_{snow} indicate drier (wetter) than normal conditions (Table 2).

2.2.4. Evaluating Performance

Trenberth and Shea (2005), Adler et al. (2008), and Yin et al. (2014) suggested that water and energy are negatively correlated during drought events. This suggests that the ratio of sensible heat to net radiation (total energy supply) during a drought is larger than the normal condition, while the residual available water ($P - ET$) to precipitation (total water supply) is usually lower than its normal condition. Based on their theoretical analysis, Liu et al. (2017) demonstrated that the ratio of the residual available water to the residual energy ($PET - ET$) is relatively low (large) during drought (wet) events relative to normal conditions. Defining this ratio as $WER = (P - ET)/(PET - ET)$, they proposed a method for examining the response of the surface water-energy fluxes to drought based on WER. It follows that the Pearson correlation coefficient (r) between WER and SZI_{snow} that can serve as a rational evaluation criterion for the performance of SZI_{snow} as a drought indicator.

However, the WER proposed by Liu et al. (2017) does not consider the influence of snow accumulation or melt on the water-energy balance. As a result, a modified version of WER (i.e., WER_{snow}) was developed in this study by incorporating SWE as follows:

$$WER_{snow} = \frac{P - ET - \Delta SWE}{PET - ET + \Delta SWE} \tag{10}$$

To ensure that the WER_{snow} is independent of the SZI and SZI_{snow} at global scales, the variables P and PET in equation (10) for each test basin were provided by the CRU data set, while the ET was obtained from the remote sensing-based GLEAM ET product. Because the monthly CRU data are at a uniform spatial resolution of 0.5°, the daily GLEAM ET data (0.25° × 0.25°) were interpolated onto monthly 0.5° × 0.5° grids to create a common resolution.

The SZI and SZI_{snow} values were also compared with observed drought evidences (streamflow as indicator for hydrological droughts and soil water storage as indicator for agricultural droughts) over 32 basins. The log-logistic distribution is also selected to standardize streamflow (provided by Pan et al., 2012), soil water storage (provided by Pan et al. (2012)), and WER_{snow} data to compute the Standardized Streamflow Index (SSI; Vicente-Serrano, López-Moreno, et al., 2012), Standardized Water Storage Index (SWSI; AghaKouchak, 2014), and Standardized Wetness Index (SWI; Liu et al., 2017), respectively. Although other three-parameter distributions, including Pearson III, lognormal, and general extreme values, were also tested for standardizing SSI, SWSI, and SWI, the test results show that the log-logistic distribution performed the best at multiple temporal scales. To evaluate the performance of SZI and SZI_{snow} in drought identification, the Pearson linear correlation between the reference indices (SSI, SWSI, and SWI) and derived SZI and SZI_{snow} was calculated. The drought and wetness threshold levels for SZI_{snow}, SZI, SSI, SWSI, and SWI are shown in Table 2 in the supporting information.

3. Results

3.1. Global Distribution of Precipitation, Snowfall, and the Water Demand

Since the effects of snow dynamics on both the water supply and demand were taken into account in the SZI_{snow}, the differences among P, P_{snow}, $\widehat{P}$, and $\widehat{P}_{snow}$ should firstly be examined. Snowfall (P_{snow}) primarily occurs at high-latitude and/or mountainous areas (Figure 4(a)), and the P_{snow} comprises more than 50% of P over polar regions and the Qinghai-Tibetan Plateau (Figure 4(b)). Snowfall builds the snowpack on the land

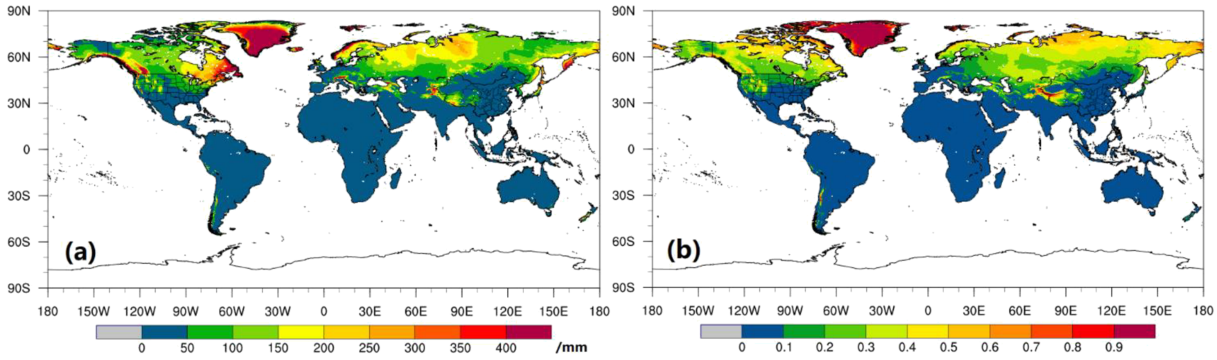

Figure 4. Global distribution of mean annual P_{snow} a and the ratio P_{snow}/P b.

surface, and melt and refreezing processes modulate the snowpack during the cold season. When the land surface warms, the accumulated snowmelts and water drains into the soil increasing soil moisture and groundwater or it drains directly into the river network. This can lead to a several-month to 1-year lag response in the soil wetness and total water storage variability.

$\widehat{P}_{snow}$ was 100–600 mm larger than $\widehat{P}$ over high-latitude regions (Figures 5(a)–5(c)) because snowpack accumulation consumes part of the water supply (i.e., goes into storage as SWE) and enhances the water demand. The ratio of $P/\widehat{P}$ is ~1.0 over most regions of the globe, except in the high-latitude areas (Figure 5(d)). In the polar region, P is 40% larger than $\widehat{P}$, which causes a water imbalance in drought modeling and characterization as it is assumed that P falls as snow on the land surface and then disappears immediately. Therefore, this may degrade the performance of SZI in drought identification over different temporal scales in cold regions. By including snow accumulation and melt over cold regions, the ratio of $P/\widehat{P}_{snow}$ is closer to 1.0 than $P/\widehat{P}$ (Figures 5(e) and 5(f)), suggesting that SZI_{snow} is better suited for representing the water balance in snow-covered regions than the SZI. Hence, the snow processes incorporated into SZI_{snow} result in a more generalized framework for drought assessment, which converges to SZI in regions without snow.

3.2. Monitoring Different Types of Droughts

To assess the performance and ability of the SZI and SZI_{snow} to monitor hydrological and agricultural droughts, the correlations between observed streamflow and soil water storage and the derived drought condition, identified by SZI and SZI_{snow}, were compared at basins across the globe.

3.2.1. Hydrological Drought

Figure 6 shows the temporal variation of correlation coefficients between SSI and SZI/SZI_{snow} for one to 48 monthly time scales. The correlation coefficients between SZI_{snow} and SSI vary from 0.26–0.99 over the 32 basins (with an average value of 0.78). The correlation coefficients are slightly lower between SZI and SSI ($0.23 \leq r \leq 0.97$; average value: $r = 0.75$). However, over the basins with the highest SWE accumulation, the correlation values between SZI_{snow} and SSI are much greater than those between SZI and SSI. For basins with minimal to no snow accumulation, the correlation coefficients are almost the same. When SSI is used as a reference for a hydrological drought (Figure S7), the SZI_{snow} exhibits larger correlation coefficients with SSI than SZI does for all four snow-dominated basins. Specifically, the performance of SZI_{snow} in identifying the 12-month scale hydrological droughts are 12.6%, 12.5%, 19.1%, and 10.5% better than SZI at Pechora, Northern Dvina, Yenisei, and Kolyma basin, respectively. The SZI_{snow} is higher correlated because snow accumulation and melt have large impacts on the seasonal cycle and temporal variability of streamflow in such regions. Since SZI only accounts for the role of the snowpack on streamflow variation for cases when snowfall immediately produces streamflow, correlations between SZI and SSI are lower where such assumptions lead to larger deviations from the SSI. Hence, the SZI_{snow} outperforms SZI for hydrological drought identification.

3.2.2. Agricultural Drought

The temporal variation of correlation coefficients between SWSI and SZI, as well as those between SWSI and SZI_{snow} for the same 32 basins is illustrated in Figure 7. The average correlation over all of the basins is

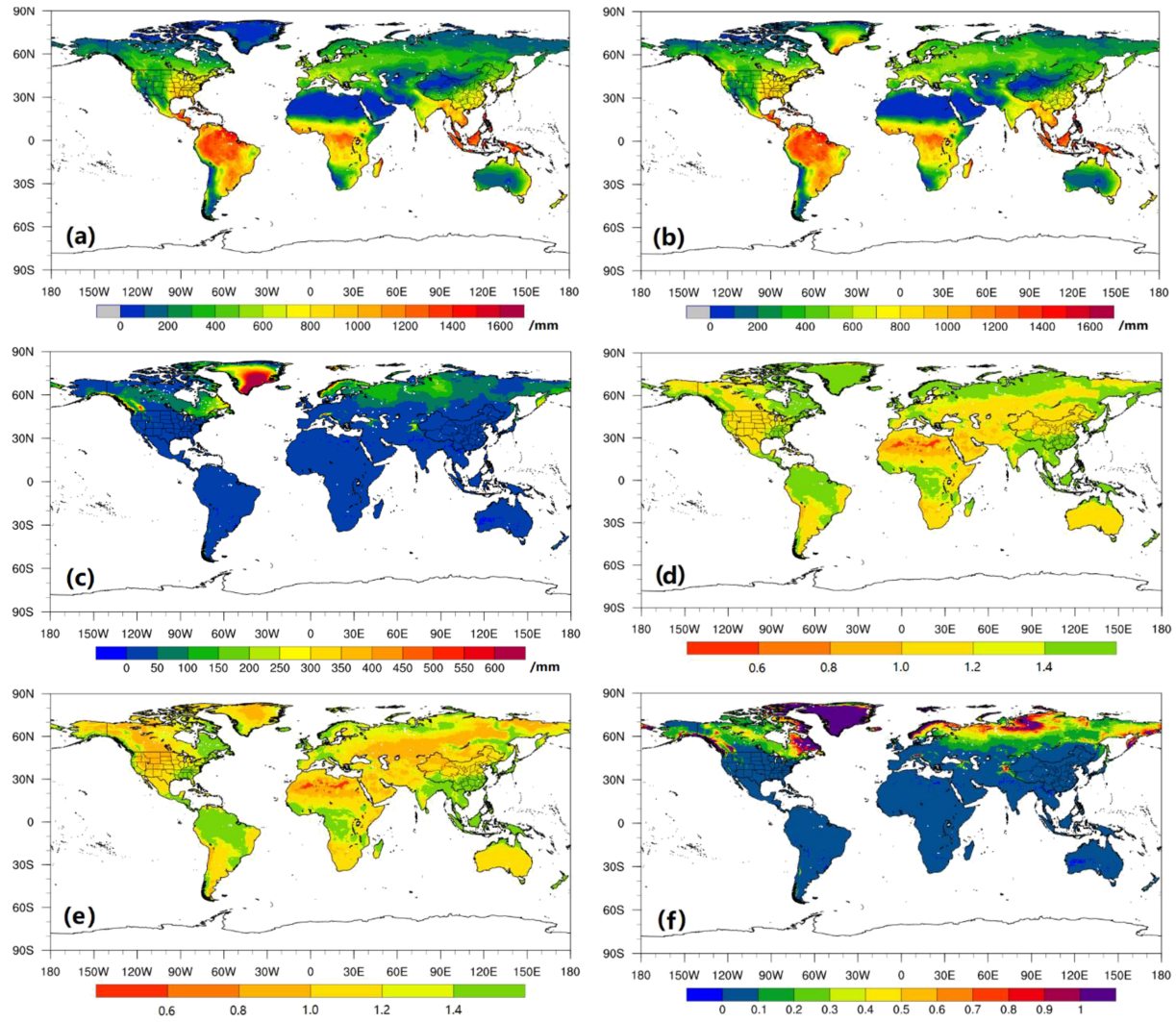

Figure 5. Global distribution of annual $\widehat{P}$ a, annual $\widehat{P}_{snow}$ b, and the annual difference between $\widehat{P}_{snow}$ and $\widehat{P}$ c, the ratio $P/\widehat{P}$ (c), the ratio $P/\widehat{P}_{snow}$ d, and the difference between $P/\widehat{P}$ and $P/\widehat{P}_{snow}$ e.

comparable for the SZI and SZI_{snow} cases (i.e., 0.46 vs. 0.50, respectively). However, for those basins receiving large amounts of SWE, the correlation coefficient associated with SZI_{snow} is higher than that of the SZI. When the SWSI is used as a reference (Figure S8), SZI_{snow} outperforms SZI for quantifying agricultural droughts. Specifically, the correlations between SZI_{snow} and SWSI are 31.4%, 18.6%, 14.3%, and 13.2% higher than those between SZI and SWSI at the 9-month scale over Pechora, Northern Dvina, Yenisei, and Kolyma basin, respectively.

Moreover, it should be noted that both the SZI and the SZI_{snow} not only can be calculated based on regional or basin averages but also for individual grid cells. To demonstrate this, we show regions experiencing drought conditions as defined in Table 2 over the heavily snow-influenced Lena, Mackenzie, Ob, Volga, and Yenisei basins (Figure S9). The results confirm our conclusions based on correlation analysis—the SZI_{snow} better characterizes hydrological and agricultural droughts in high-latitude and/or high-elevation regions with a deep snowpack. Also, the SZI_{snow} identifies the water-energy residual during drought events (which is one of the most important indicators of multiple categories drought events) in all five basins at grid cell level.

3.3. Global Evaluation Using the SWI

To further understand the effects of including snow dynamics in drought modeling at the global scale, the latitudinal and temporal variations of the differences between the correlation coefficients between SZI_{snow}

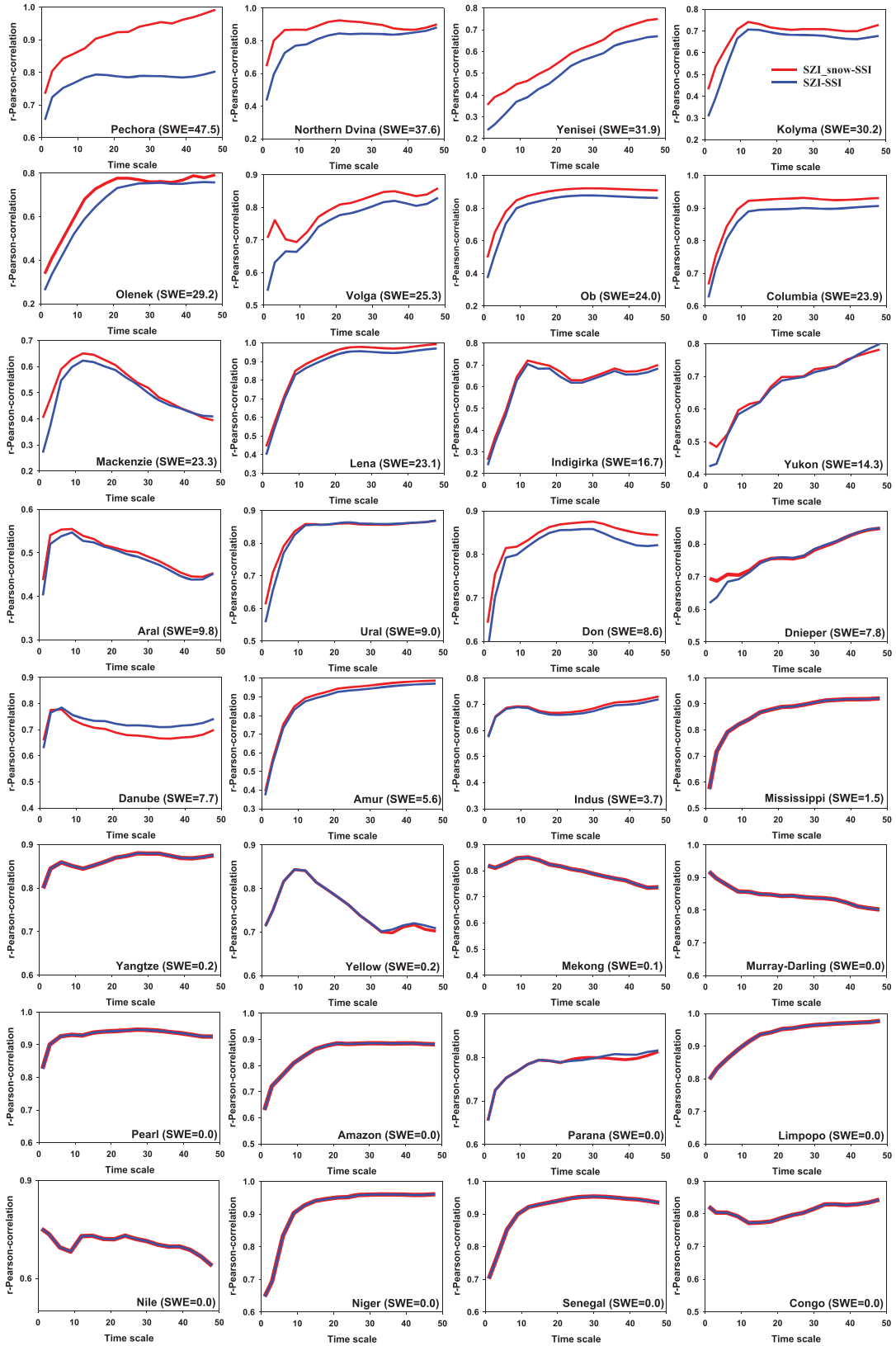

Figure 6. Pearson correlation coefficients for time scales from 1–48 months when SZI_{snow} and SZI are correlated with SSI at 32 global basins over 1984–2006. The SWE is long-term annual mean value in millimeter. SWE = snow water equivalent; SSI = standardized Streamflow index; SZI = standardized moisture anomaly index.

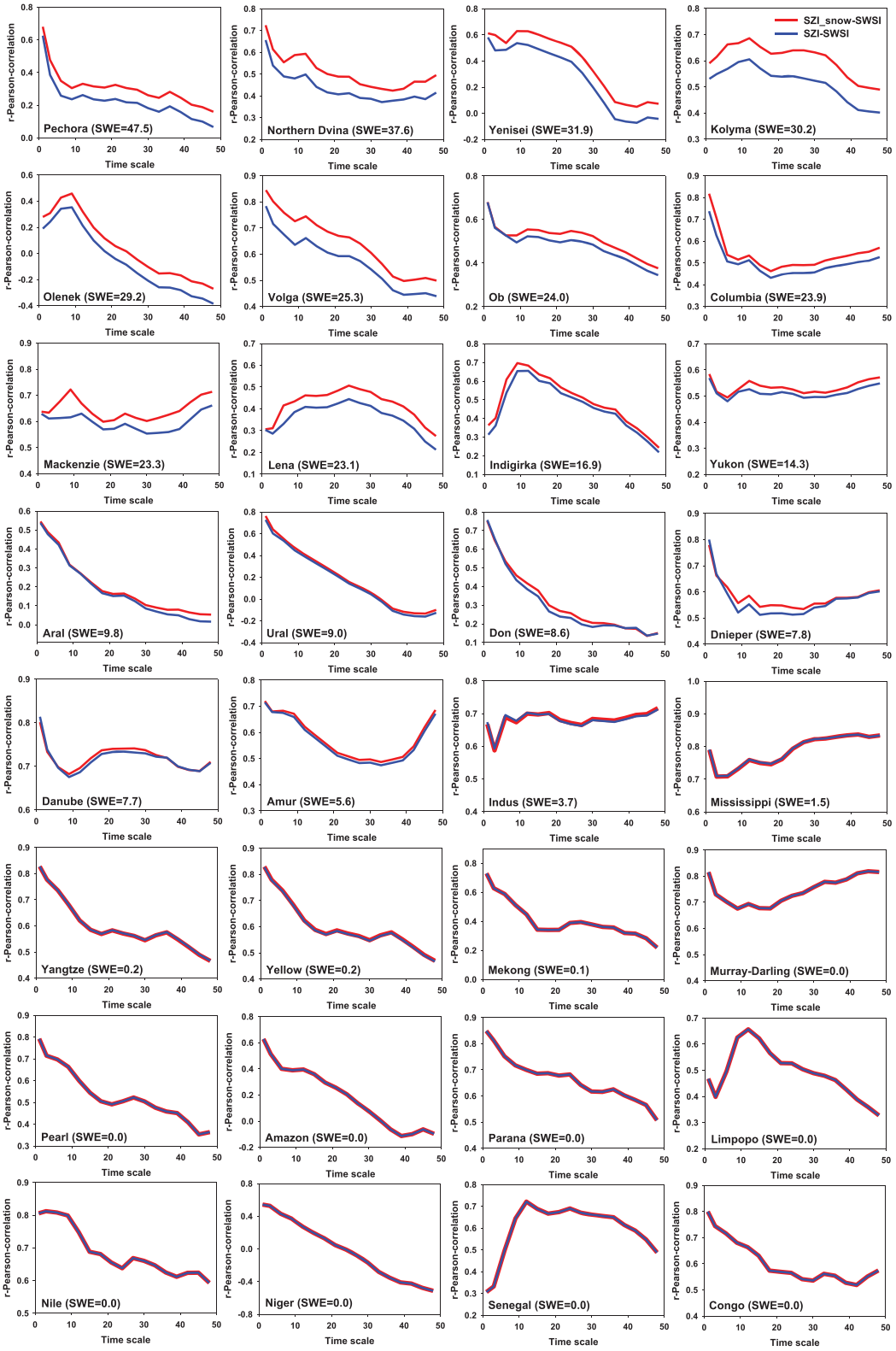

Figure 7. Pearson correlation coefficients for time scales from 1–48 months when SZI_{snow} and SZI are correlated with SWSI at 32 global basins over 1984–2006. The SWE is long-term annual mean value in millimeter. SWE = snow water equivalent; SSI = standardized Streamflow index; SZI = standardized moisture anomaly index; SWSI = standardized water storage index.

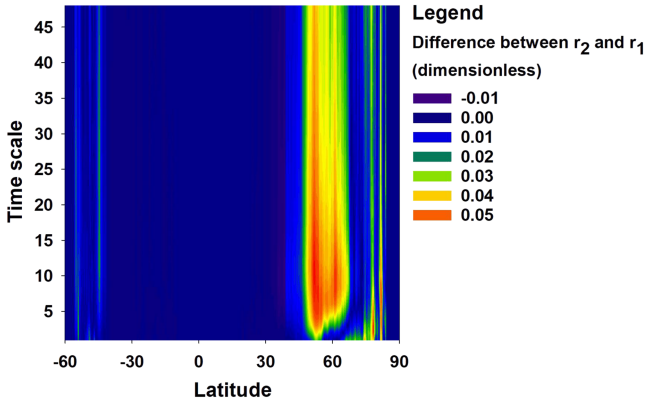

Figure 8. Difference between two correlation coefficients ($r_2 - r_1$), where r_2 is the correlation between SZI_{snow} and SWI and r_1 is the correlation between SZI and SWI. The array is shown for latitudes 60°S–90°N and 1- to 48-month time scales.

and SWI are compared to the correlation coefficients between SZI and SWI, which is taken as reference in this case (Figure 8). The difference between the two sets of correlation coefficients are generally positive, and the highest values were found between 50°N–65°N, suggesting that SZI_{snow} performs better than SZI, particularly in this 15° latitudinal range. In contrast, the correlation coefficient values are nearly identical in the mid- and low-latitude regions where snow impacts the drought characterization less. Although performance depends on latitude, SZI_{snow} shows the largest improvements over SZI at 3- to12-month scales, which is largely attributed to the fact that *WER* is most sensitive to snowmelt/accumulation within one water year (but insensitive to snow dynamics shorter than the 3-month scale).

Maps of correlations between SZI_{snow} and SWI (left column), correlations between SZI and SWI (middle column), and the differences between them (right column) in the Arctic region are shown in Figure 9 over a variety of temporal scales. The correlations vary spatially for the 6-, 9-, 12-, and 15-month time scales (from top to bottom in Figure 9). Generally, the differences between correlations are positive for most Arctic regions across all time scales, highlighting the value of considering snow dynamics in SZI_{snow}. As the time scale increases from 6–12 months, this improvement also increases (Figure 9). Overall, the addition of snow processes improves upon SZI performance across the Arctic, particularly at the 6- to 12-month time scales, although this improvement varies spatially across the time scales considered here (Figure 9).

4. Discussion

4.1. Advantages of SZI_{snow}

The development of drought indices for varied applications is essential to drought prediction/mitigation and water resources management (Liu et al., 2015, 2016). However, it is still difficult to establish a universal drought index that can monitor and identify all types of droughts. Nonetheless, the SZI_{snow}, resulting from the incorporation of snow dynamics into the SZI, addresses deficiencies in the SZI as well as the PDSI and SPEI that are important for identifying, monitoring, and quantifying agricultural and hydrological droughts specifically in those climatic regions with distinct snowmelt and snow accumulation/wet seasons. Because the SZI_{snow} requires information about *P*, SWE, *RO*, *ET*, and changes in soil water storage, which can be easily obtained from LSMs through Land Data Assimilation Systems or Coupled Model Intercomparison Project, it is suitable for regional comparisons using distributed or gridded hydrometeorological data sets without any additional information required. It should be noted that the performance of the SZI_{snow} is equal to the performance of the SZI in areas that are snow free.

4.2. Limitations of SZI_{snow}

The main limitation of SZI_{snow} is that its computation is more complex and difficult than the computation of the standardized precipitation index, the SPEI, and the SZI as it adds several variables associated with snowmelt and accumulation processes. Although the operational application of the SZI_{snow} is important for improvement of mitigation and disaster reduction strategies related to droughts, at its current stage, the SZI_{snow} cannot yet be used for operational application due to its complexity. Therefore, a collaboration between our researchers and operational agencies/centers (e.g., United States Drought Monitor, China Meteorological Administration) to test operational feasibility of the SZI_{snow} is needed in the future. Another limitation of the SZI_{snow} is that its calculation requires long-term climatic and hydrologic records, which makes it unsuitable for short-term drought identification.

Moreover, because the establishment of SZI_{snow} is based on GLDAS or other similar LSMs output, the performance and quality of these models directly determines the accuracy of SZI_{snow} in drought characterization. Since the GLDAS or LSM inevitably have uncertainties including forcing data errors, model structure deficiencies, and model parameters errors, an urgent issue that needs to be addressed in the future becomes how to minimize the effects of the uncertainties associated with input data for SZI_{snow}. Despite

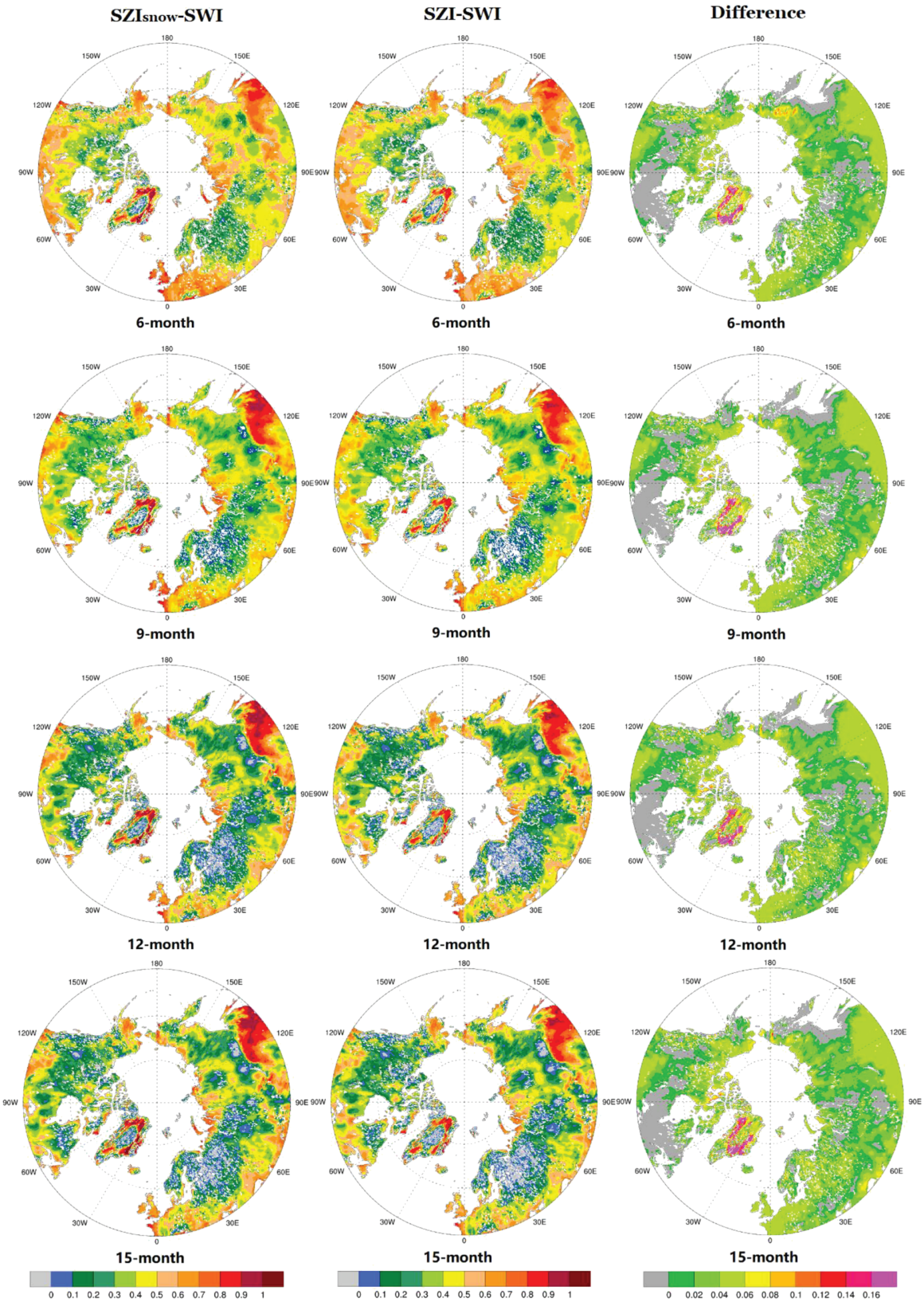

Figure 9. Spatial distribution of correlation coefficients between SZI_{snow} and SWI (left column) and between SZI and SWI (middle column), and the differences between the two maps (left column - middle column) in the Arctic for various temporal scales. SZI = standardized moisture anomaly index; SWI = standardized wetness index.

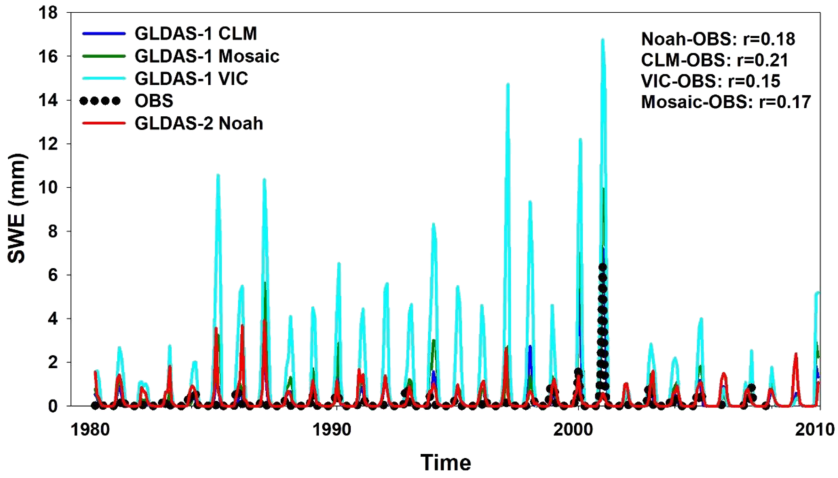

Figure 10. Comparison of monthly-averaged SWE OBS and fields from GLDAS-2 Noah LSM and GLDAS-1 CLM, mosaic, and VIC LSMs over northeastern China for the green dots in Figure 1(f) (the simulations and observations at different points are averaged to a mean value). CLM = community land model; GLDAS; SWE = snow water equivalent; OBS = observations; VIC = variable infiltration capacity; LSM = land surface model.

such limitations, the SZI_{snow} provides a better tool for monitoring water resources (dry and wet spells), particularly in high-latitude and high-altitude regions with thick snowpack. Although the SZI_{snow} is a physically based multiscalar and multicategory drought index, averaging across a variety of topographic features over large areas, the uncertainty of precipitation input, and so forth can potentially cause unrealistic water budgets on large scales and introduce systematic biases in drought monitoring.

4.3. Uncertainties of Snow Data From GLDAS Products

The representation of the snow processes in the GLDAS product is crucial because snow has a large influence on water-energy fluxes on the land surface, thereby affecting the accuracy of drought identification. For instance, the high albedo of snow determines the amount of solar radiation absorbed by the land surface, which influences the turbulent exchanges of water and energy between the land and the atmosphere. The hydrological application of GLDAS also depends largely on the accurate representation of snow processes because the hydrology of cold regions is heavily influenced by snow accumulation and melt (Bales et al., 2006). However, uncertainty remains with respect to the representation of snow on the ground in the GLDAS product, as evidenced by the low correlations between the SWE (or SNWD) GLDAS fields and observations in certain regions (Broxton et al., 2016).

Although we showed that the GLDAS-2 provides reasonable estimates of SWE and SNWD across several regions of the world (Figure 1), large uncertainties exists in some parts of northeastern China. A comparison between the SWE observations and GLDAS fields from four LSMs over northeastern China (the green dots in Figure 1(f)) is shown in Figure 10. For these locations, the four LSMs do not capture the temporal variations of the SWE observations well since correlation coefficients are small ($0.15 \leq r \leq 0.21$). The long-term annual mean observed SWE is 1.26 mm, while the SWE from GLDAS-2 Noah and GLDAS-1 CLM, VIC, and Mosaic are 3.39, 3.14, 13.66, and 5.33 mm, respectively, indicating large uncertainties relative to the observations and among the various LSM estimates. The SWE estimates from the four LSMs are substantially higher than observed. The reason for these uncertainties remains unclear and needs further investigation from many aspects such as forcing data, model structures, and model parameters. Besides, there are uncertainties and biases associated with the observed SWE data as well (Meyer et al., 2012). Nonetheless, a large spatial disparity exists between the observations and GLDAS SWE fields from the four LSMs.

In practical application, not only SWE variability but also its amount has large impact on the SZI. Generally, snow amount measurement has errors due to blowing snow caused by wind, vegetation density, and topographic slope effect. For simulated and satellite retrieved snow amount, there are large uncertainties and errors as snow dynamics included in LSMs is not well understood and remote sensing techniques is limited in snow cover conditions. Besides SWE, an additional measure can be used is SNWD (volume). In general,

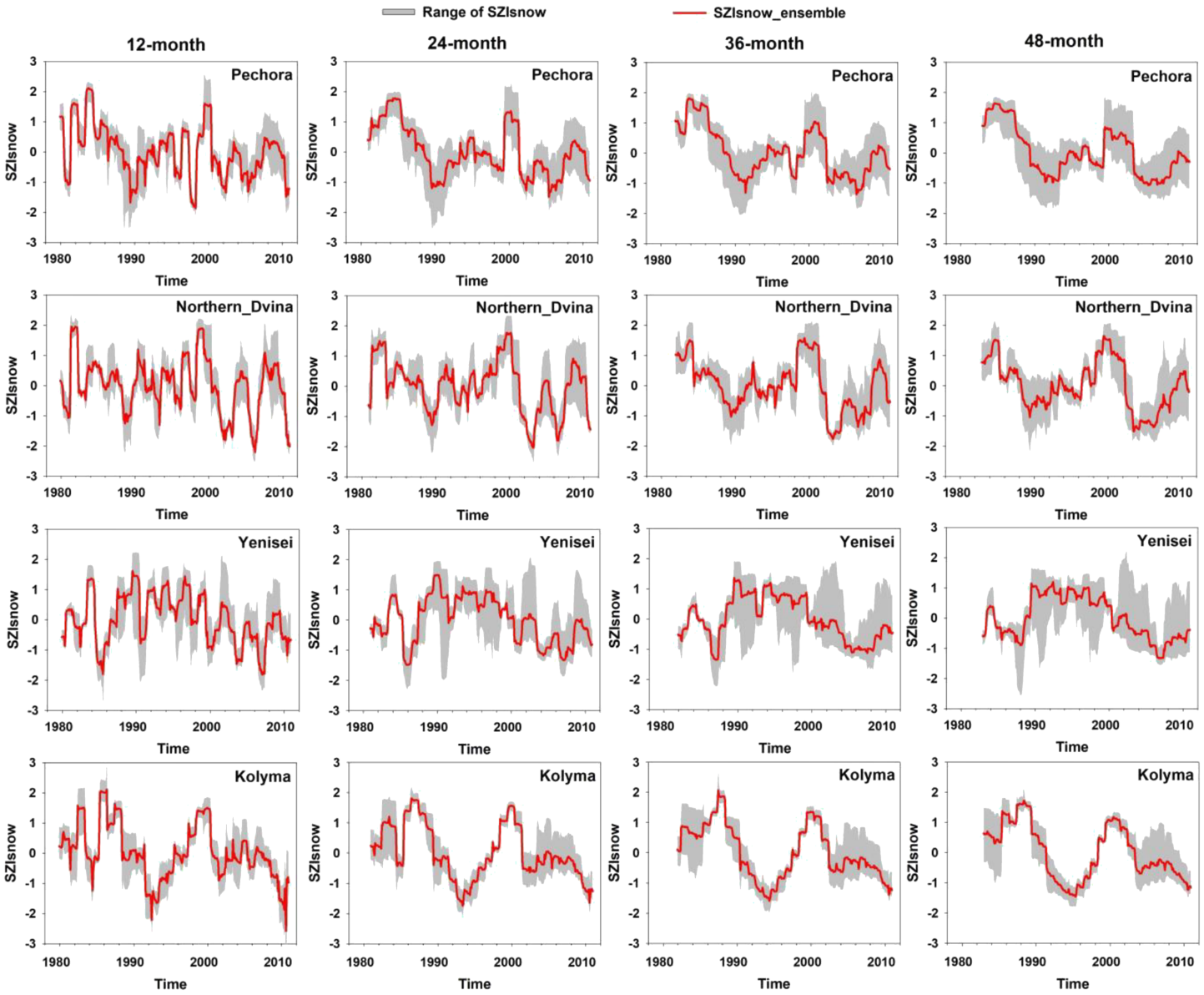

Figure 11. Basin-averaged SZI_{snow} computed using the mean (red lines) and range of SZI_{snow} values (gray shading) from the individual LSMs at 12-, 24-, 36-, and 48-month scales. SZI = standardized moisture anomaly index; LSM = land surface model.

SWE can be derived from SNWD when snow density is known. However, snow density varies with snow age, which is a very difficult to measure. Such a conversion brings an extra challenge when SNWD is used. Nevertheless, it should be noted that both snow variability and amount uncertainties (e.g., SWE, SNWD) have a large impact on SZI calculation and analysis and need to be further investigated in the future. We simply used the GLDAS-1 products from three models (CLM2.0, Mosaic, and VIC4.0.4) and GLDAS-2 (Noah) to quantify the uncertainty associated with SZI_{snow} since snowfall and SWE are used in the calculation. Figure 11 provides a comparison of the mean and range of SZI_{snow} values calculated across the four GLDAS products for the selected snow-dominated basins (rows) at 12-, 24-, 36-, and 48-month time scales (columns). Using the GLDAS products, large uncertainties exist across all four basins (Figure 11). As the time scales increase, the uncertainties become larger, again, depending on the basin and time scale (Figure 11).

Despite that the GLDAS products have relatively large uncertainties when the result from low quality meteorological forcing data (in particular precipitation data) are used to run LSMs, hydrological, and

agricultural studies over regions that lack observations still would benefit from GLDAS products. We recognize that the uncertainty associated with P_{snow} and P_{rain} data influences the results of SZI_{snow}. However, despite uncertainties in the GLDAS snow simulation, theoretically, the accuracy of the input water budget components does not influence the conceptual or technical improvement of the SZI_{snow}, since the impact of snow dynamics is considered for both water supply and demand in our drought characterization. As soon as additional GLDAS and reanalysis products including satellite retrievals become available, a multisystem and multimodel SZI_{snow} along with uncertainty estimates will be calculated to enhance its robustness and reliability. This ongoing work will be reported in the future.

5. Conclusions

The SZI_{snow}, as introduced in this work, overcomes the limitations of the SZI by using components of the water-energy budget from the GLDAS-2 Noah LSM to incorporate the influence of snow on both the water supply and demand in drought characterization. Although we computed the SZI_{snow} using GLDAS products, the general framework for calculating the drought index from other data sets is possible given that reasonable estimates of the required water and energy budget variables are available. Furthermore, the SZI_{snow} can be applied at multiple spatial (i.e., grid cell to global scales) and temporal scales (1 to 48 months) as demonstrated herein. Therefore, this index provides the community not only with a global drought identification data set, but also a complementary methodology for characterizing and monitoring hydrological and agricultural droughts across both snow-covered and snow-free regions.

The application of SZI_{snow} to snow-covered regions is particularly important given that the snow impacts the surface water balance and thus affect the onset, duration, intensity, and spatial extent of drought at varied time scales. In this study, we demonstrated the usefulness of SZI_{snow} for drought monitoring at multiple temporal scales across the globe, particularly in snow-covered basins. Except for some parts of northeastern China, the GLDAS-2 Noah LSM snowfields performed well across most regions considered relative to in situ SWE and SNWD observations. This indicates that the GLDAS-2 Noah LSM product is qualified for use in global application of the SZI_{snow}. In the 32 basins specifically examined herein, the SZI_{snow} had larger correlations with the observed changes in hydrological and agricultural droughts than the SZI for the basins with a deep snowpack.

Although the SZI_{snow} requires more information than the SZI to additionally account for snowpack accumulation and melt processes in the water budget, this additional complexity yields meaningful improvements in snow-covered regions. As demonstrated herein, the more that a basin is influenced by snow, the more worthwhile it becomes to complement the SZI with the SZI_{snow}. In addition, it is not surprising that the SWI is more consistent with the SZI_{snow} than the SZI over high-latitude and high-elevation cold regions, suggesting the imporoved value of the SZI_{snow} for identifying, monitoring, and characterizing drought events. The theoretical improvement that the SZI_{snow} has over SZI occurs since the former accounts for snow processes in drought identification, and this should be reflected assuming that reasonable values are input for the water-energy budget (as demonstrated with GLDAS-2 Noah LSM fields herein).

Finally, we note that most of the existing Drought Early Warning Systems (DEWSs) focus on the hazard component of drought monitoring, without accounting for snow processes (e.g., Wilhite et al., 2000; Hao et al., 2014, WMO and GWP, 2016, and therein). The existing DEWSs can benefit from incorporating snow information especially in snow-dominated regions. This paper offers a possible pathway forward to improve exiting DEWSs through incorporating SZI_{snow}.

Acknowledgments
This work is jointly supported by the National Natural Science Foundation of China (41877150 and 51609111), the National Key R&D Program of China (2017YFC0403600), the Strategic Priority Research Program of Chinese Academy of Sciences (XDA20100102), and the Natural Science Foundation of Qinghai Province in China (2018-ZJ-936Q). Amir AghaKouchak and Laurie S. Huning were supported by the National Aeronautics and Space Administration (NNX16AO56G) and the National Oceanic and Atmospheric Administration MAPP Program. The GLDAS data are downloaded via the Goddard Earth Sciences Data and Information Services Center website (http://disc.sci.gsfc.nasa.gov/hydrology/data-holdings). The observed daily SNWD and SWE data in western United States and Alaska are obtained from Snowpack Telemetry network Natural Resources Conversation Service (http://www.wcc.nrcs.usda.gov/nwcc/inventory). The observed monthly SNWD data in the Xinjiang Province is provided by the Xinjiang Meteorological Bureau (http://www.xjqx.cn/). The observed monthly SNWD and SWE data in eastern China are obtained from the National Meteorological Information Center of China (http://data.cma.cn/site/index.html). The monthly climatic observations from CRU TS 4.01 are available from http://www.cru.uea.ac.uk/cru/data/hrg/. The global daily GLEAM *ET* product is downloaded from https://www.gleam.eu/. The observed hydrologic data developed for 32 global basins are provided by Pan et al. (2012), Xu et al. (2013), and Liu et al. (2017). A more detailed discussion of the methodology and results can be found in the supporting information (Chen et al., 1996; Dai et al., 2003; Koren et al., 1999; Koster & Suarez, 1994; Liang et al., 1994; Pan et al., 2012; Sheffield et al., 2006). Computer codes and data for calculating the SZI_{snow} will be provided as well as the global SZI_{snow} data set presented in this study.

References

Adler, R. F., Gu, G. J., Wang, J. J., Huffman, G. J., Curtis, S., & Bolvin, D. (2008). Relationships between global precipitation and surface temperature on interannual and longer timescales (1979-2006). *Journal of Geophysical Research*, *113*, D22104. https://doi.org/10.21029/22008JD010536

AghaKouchak, A. (2014). A baseline probabilistic drought forecasting framework using standardized soil moisture index: Application to the 2012 United States drought. *Hydrology and Earth System Sciences*, *18*, 2485–2492. https://doi.org/10.5194/hess-18-2485-2014

AghaKouchak, A., Farahmand, A., Melton, F. S., Teixeira, J., Anderson, M. C., Wardlow, B. D., & Hain, C. R. (2015). Remote sensing of drought: Progress, challenges and opportunities. *Reviews of Geophysics*, *53*, 452–480. https://doi.org/10.1002/2014RG000456

Allen, R. G., Pereira, L. S., Raes, D., & Smith, M., (1998). Crop evapotranspiration—Guidelines for computing crop water requirements. FAO Irrigation and Drainage Paper 56. Food and Agriculture Organization of the United Nations, Rome, Italy, pp. 300.

Arheimer, B., Donnelly, C., & Lindström, G. (2017). Regulation of snow-fed rivers affects flow regimes more than climate change. *Nature Communications*, *8*(1), 62. https://doi.org/10.1038/s41467-017-00092-8

Bales, R. C., Molotch, N. P., Painter, T. H., Dettinger, M. D., Rice, R., & Dozier, J. (2006). Mountain hydrology of the western United States. *Water Resources Research*, *42*, W08432. https://doi.org/10.1029/2005WR004387

Barnett, T. P., Adam, J. C., & Lettenmaier, D. P. (2005). Potential impacts of a warming climate on water availability in snow-dominated regions. *Nature*, *438*(17), 303–309. https://doi.org/10.1038/nature04141

Beguería, S., Vicente-Serrano, S. M., Reig, F., & Latorre, B. (2014). Standardized precipitation evapotranspiration index (SPEI) revisited: Parameter fitting, evapotranspiration models, tools, datasets and drought monitoring. *International Journal of Climatology*, *34*, 3001–3023. https://doi.org/10.1002/joc.3887

Broxton, P. D., Zeng, X. B., & Dawson, N. (2016). Why do global reanalyses and land data assimilation products underestimate snow water equivalent? *Journal of Hydrometeorology*, *17*, 2743–2761. https://doi.org/10.1175/JHM-D-16-0056.1

Chen, F., Mitchell, K., Schaake, J., Xue, Y., Pan, H., Koren, V., et al. (1996). Modeling of land-surface evaporation by four schemes and comparison with FIFE observations. *Journal of Geophysical Research*, *101*(D3), 7251–7268. https://doi.org/10.1029/95JD02165

Chen, Y., Yang, K., Qin, J., Zhao, L., Tang, W., & Han, M. (2013). Evaluation of AMSR-E retrievals and GLDAS simulations against observations of a soil moisture network on the central Tibetan plateau. *Journal of Geophysical Research: Atmospheres*, *118*, 4466–4475. https://doi.org/10.1002/jgrd.50301

Dai, A. G. (2011). Characteristics and trends in various forms of the Palmer drought severity index during 1900–2008. *Journal of Geophysical Research*, *116*, D12115. https://doi.org/10.1029/2010JD015541

Dai, A. G. (2013). Increasing drought under global warming in observations and models. *Nature Climate Change*, *3*, 52–58. https://doi.org/10.1038/NCLIMATE1633

Dai, Y., Zeng, X. B., Dickinson, R. E., Baker, I., Bonan, G. B., Bosilovich, M. G., et al. (2003). The common land model. *Bulletin of the American Meteorological Society*, *84*(8), 1013–1024. https://doi.org/10.1175/BAMS-84-8-1013

Hao, Z., AghaKouchak, A., Nakhjiri, N., & Farahmand, A. (2014). Global integrated drought monitoring and prediction system. *Scientific Data*, *1*(1), 1–10. https://doi.org/10.1038/sdata.2014.1

Hao, Z. C., & AghaKouchak, A. (2013). Multivariate standardized drought index: A parametric multi-index model. *Advances in Water Resources*, *57*, 12–18. https://doi.org/10.1016/j.advwatres.2013.03.009

Harris, I., Jones, P. D., Osborn, T. J. & Lister, D. H. (2014). Updated high-resolution grids of monthly climatic observations—The CRU TS3.10 Dataset. *International Journal of Climatology, 34*, 623–642. https://doi.org/10.1002/joc.3711

Huning, L., & AghaKouchak, A. (2018). Mountain snowpack response to different levels of warming. *Proceedings of the National Academy of Sciences of the United States of America*, *115*(43), 10,932–10,937. https://doi.org/10.1073/pnas.1805953115

Jenicek, M., Seibert, J., Zappa, M., Staudinger, M., & Jonas, T. (2016). Importance of maximum snow accumulation for summer low flows in humid catchments. *Hydrology and Earth System Sciences*, *20*, 859–874. https://doi.org/10.5194/hess-20-859-2016

Jones, P. D., & Moberg, A. (2003). Hemispheric and large-scale surface air temperature variations: An extensive revision and an update to 2001. *Journal of Climate*, *16*, 206–223. https://doi.org/10.1175/1520-0442(2003)016<0206:HALSSA>2.0.CO;2

Koren, V., Schaake, J., Mitchell, K., Duan, Q. Y., Chen, F., & Baker, J. M. (1999). A parameterization of snowpack and frozen ground intended for NCEP weather and climate models. *Journal of Geophysical Research*, *104*, 19,569–19,585. https://doi.org/10.1029/1999JD900232

Koster, R., & Suarez, M. (1994). The components of the SVAT scheme and their effects on a GCM's hydrological cycle. *Advances in Water Resources*, *17*, 61–78. https://doi.org/10.1016/0309-1708(94)90024-8

Liang, X., Lettenmaier, D. P., Wood, E. F., & Burges, S. J. (1994). A simple hydrologically based model of land surface water and energy fluxes for GCMs. *Journal of Geophysical Research*, *99*, 14,415–14,428. https://doi.org/10.1029/94JD00483

Liu, M. X., Xu, X. L., Xu, C. H., Sun, A. Y., Wang, K. L., Scanlon, B. R., & Zhang, L. (2017). A new drought index that considers the joint effects of climate and land surface change. *Water Resources Research*, *53*, 3262–3278. https://doi.org/10.1002/2016WR020178

Liu, Y., Ren, L. L., Ma, M. W., Yang, X. L., Yuan, F., & Jiang, S. H. (2016). An insight into the Palmer drought mechanism based indices: Comprehensive comparison of their strengths and limitations. *Stochastic Environmental Research and Risk Assessment*, *30*(1), 119–136. https://doi.org/10.1007/s00477-015-1042-4

Liu, Y., Yang, X. L., Ren, L. L., Yuan, F., Jiang, S. H., & Ma, M. W. (2015). A new physically based self-calibrating Palmer drought severity index and its performance evaluation. *Water Resources Management*, *29*(13), 4833–4847. https://doi.org/10.1007/s11269-015-1093-9

Margulis, S. A., Cortés, G., Girotto, M., Huning, L. S., Li, D., & Durand, M. (2016). Characterizing the extreme 2015 snowpack deficit in the Sierra Nevada (USA) and the implications for drought recovery. *Geophysical Research Letters*, *43*, 6341–6349. https://doi.org/10.1002/2016GL068520

Martens, B., Miralles, D. G., Lievens, H., van der Schalie, R., de Jeu, R. A. M., Fernández-Prieto, D., et al. (2017). GLEAM v3: Satellite-based land evaporation and root-zone soil moisture. *Geoscientific Model Development*, *10*(5), 1903–1925. https://doi.org/10.5194/gmd-10-1903-2017

McEvoy, D. J., Huntington, J. L., Abatzoglou, J. T., & Edwards, L. M. (2012). An evaluation of multiscalar drought indices in Nevada and eastern California. *Earth Interactions*, *16*, 1–18. https://doi.org/10.1175/2012EI000447.1

McKee, T. B., Doesken, N. J., & Kleist, J. (1993). The relationship of drought frequency and duration to time scales. *In Proceedings of the 8th Conference of Applied Climatology,* 17–22 January, Anaheim, CA. American Meteorological Society, Boston, MA. 179–184.

Meyer, J. D. D., Jin, J. M., & Wang, S. Y. (2012). Systematic patterns of the inconsistency between snow water equivalent and accumulated precipitation as reported by the snowpack telemetry network. *Journal of Hydrometeorology*, *13*, 1970–1976. https://doi.org/10.1175/JHM-D-12-066.1

Miralles, D. G., Holmes, T. R. H., de Jeu, R. A. M., Gash, J. H., Meesters, A. G. C. A., & Dolman, A. J. (2011). Global land-surface evaporation estimated from satellite-based observations. *Hydrology and Earth System Sciences*, *15*, 453–469. https://doi.org/10.5194/hess-15-453-2011

Mishra, A. K., & Singh, V. P. (2010). A review of drought concepts. *Journal of Hydrology*, *391*, 202–216. https://doi.org/10.1016/j.jhydrol.2010.07.012

Mu, Q. Z., Zhao, M. S., Kimball, J. S., McDowell, N. G., & Running, S. W. (2013). A remotely sensed global terrestrial drought severity index. *Bulletin of the American Meteorological Society*, *94*, 83–98. https://doi.org/10.1175/BAMS-D-11-00213.1

Palmer, W. C. (1965). *Meteorological drought. Research Paper, 45* (Vol. 58). Washington, DC: United States weather bureau.

Pan, M., Sahoo, A. K., Troy, T. J., Vinukollu, R. K., Sheffield, J., & Wood, E. F. (2012). Multisource estimation of long-term terrestrial water budget for major global river basins. *Journal of Climate*, *25*(9), 3191–3206. https://doi.org/10.1175/JCLI-D-11-00300.1

Potopová, V., Boroneant, C., Možný, M., & Soukup, J. (2016). Driving role of snow cover on soil moisture and drought development during the growing season in the Czech Republic. *International Journal of Climatology*, *36*, 3741–3758. https://doi.org/10.1002/joc.4588

Rodell, M., Houser, P. R., Jambor, U., Gottschalck, J., Mitchell, K., Meng, C. J., et al. (2004). The global land data assimilation system. *Bulletin of the American Meteorological Society*, *85*(3), 381–394. https://doi.org/10.1175/BAMS-85-3-381

Sheffield, J., Goteti, G., & Wood, E. F. (2006). Development of a 50-yr high-resolution global dataset of meteorological forcings for land surface modeling. *Journal of Climate*, *19*(13), 3088–3111. https://doi.org/10.1175/JCLI3790.1

Sheffield, J., & Wood, E. F. (2007). Characteristics of global and regional drought, 1950–2000: Analysis of soil moisture data from off-line simulation of the terrestrial hydrologic cycle. *Journal of Geophysical Research*, *112*, D17115. https://doi.org/10.1029/2006JD008288

Sheffield, J., & Wood, E. F. (2008). Projected changes in drought occurrence under future global warming from multi-model, multi-scenario, IPCC AR4 simulations. *Climate Dynamics*, *31*, 79–105. https://doi.org/10.1007/s00382-007-0340-z

Sheffield, J., Wood, E. F., & Roderick, M. L. (2012). Little change in global drought over the past 60 years. *Nature*, *491*(7424), 435–438. https://doi.org/10.1038/nature11575

Stagge, J. H., Kingston, D. G., Tallaksen, L. M., & Hannah, D. M. (2017). Observed drought indices show increasing divergence across Europe. *Scientific Reports*, *7*(1), 1–10. https://doi.org/10.1038/s41598-017-14283-2

Stagge, J. H., Kohn, I., Tallaksen, L. M., & Stahl, K. (2015). Modeling drought impact occurrence based on meteorological drought indices in Europe. *Journal of Hydrology*, *530*, 37–50. https://doi.org/10.1016/j.jhydrol.2015.09.039

Stagge, J. H., Tallaksen, L. M., Gudmundsson, L., Van Loon, A. F., & Stahl, K. (2015). Candidate distributions for climatological drought indices (SPI and SPEI). *International Journal of Climatology*, *35*, 4027–4040. https://doi.org/10.1002/joc.4267

Stagge, J. H., Tallaksen, L. M., Gudmundsson, L., Van Loon, A. F., & Stahl, K. (2016). Response to comment on "candidate distributions for climatological drought indices (SPI and SPEI)". *International Journal of Climatology*, *36*, 2132–2138. https://doi.org/10.1002/joc.4564

Staudinger, M., Stahl, K., & Seibert, J. (2014). A drought index accounting for snow. *Water Resources Research*, *50*, 7861–7872. https://doi.org/10.1002/2013WR015143

Trenberth, K. E., Dai, A. G., van der Schrier, G., Jones, P. D., Barichivich, J., Briffa, K. R., & Sheffield, J. (2014). Global warming and changes in drought. *Nature Climate Change*, *4*, 17–22. https://doi.org/10.1038/nclimate2067

Trenberth, K. E., & Shea, D. J. (2005). Relationships between precipitation and surface temperature. *Geophysical Research Letters*, *32*, L14703. https://doi.org/10.11029/12005GL022760

van der Schrier, G., Barichivich, J., Briffa, K. R., & Jones, P. D. (2013). A scPDSI-based global data set of dry and wet spells for 1901–2009. *Journal of Geophysical Research: Atmospheres*, *118*, 4025–4048. https://doi.org/10.1002/jgrd.50355

van der Schrier, G., Jones, P. D., & Briffa, K. R. (2011). The sensitivity of the PDSI to the Thornthwaite and penman-Monteith parameterizations for potential evapotranspiration. *Journal of Geophysical Research*, *116*, D03106. https://doi.org/10.1029/2010JD015001

Vicente-Serrano, S. M., Beguería, S., & López-Moreno, J. I. (2010). A multiscalar drought index sensitive to global warming: The standardized precipitation evapotranspiration index. *Journal of Climate*, *23*(7), 1696–1718. https://doi.org/10.1175/2009JCLI2909.1

Vicente-Serrano, S. M., Beguería, S., & López-Moreno, J. I. (2012). Comment on "characteristics and trends in various forms of the Palmer drought severity index (PDSI) during 1900–2008" by Aiguo Dai. *Journal of Geophysical Research*, *116*, D19112. https://doi.org/10.1029/2011JD016410

Vicente-Serrano, S. M., Lopez-Moreno, J., Beguería, S., Lorenzo-Lacruz, J., Sanchez-Lorenzo, A., García-Ruiz, J., et al. (2014). Evidence of increasing drought severity caused by temperature rise in southern Europe. *Environmental Research Letters*, *9*, 044001. https://doi.org/10.1088/1748-9326/9/4/044001

Vicente-Serrano, S. M., López-Moreno, J. I., Beguería, S., Lorenzo-Lacruz, J., Azorin-Molina, C., & Morán-Tejeda, E. (2012). Accurate computation of a streamflow drought index. *Journal of Hydraulic Engineering*, *17*, 318–332. https://doi.org/10.1061/(ASCE)HE.1943-5584.0000433

Wang, F., Wang, L., Koike, T., Zhou, H., Yang, K., Wang, A., & Li, W. (2011). Evaluation and application of a fine-resolution global data set in a semiarid mesoscale river basin with a distributed biosphere hydrological model. *Journal of Geophysical Research*, *116*, D21108. https://doi.org/10.1029/2011JD015990

Wang, K. C., Dickinson, R. E., & Liang, S. (2012). Global atmospheric evaporative demand over land from 1973 to 2008. *Journal of Climate*, *25*, 8353–8361. https://doi.org/10.1175/JCLI-D-11-00492.1

Wang, W., Cui, W., Wang, X. J., & Chen, X. (2016). Evaluation of GLDAS-1 and GLDAS-2 forcing data and Noah model simulations over China at the monthly scale. *Journal of Hydrometeorology*, *17*, 2815–2833. https://doi.org/10.1175/JHM-D-15-0191.1

Wells, N., Goddard, S., & Hayes, M. J. (2004). A self-calibrating Palmer drought severity index. *Journal of Climate*, *17*, 2335–2351. https://doi.org/10.1175/1520-0442(2004)017<2335:ASPDSI>2.0.CO;2

Wilhite, D. A., Sivakumar, M. V. K., & Wood, D. A. (2000). Early warning systems for drought preparedness and drought management. Proceedings of an Expert Group Meeting held in Lisbon, Portugal, 5-7 September 2000. Geneva, Switzerland: World Meteorological Organization.

World Meteorological Organization (WMO), & Global Water Partnership (GWP) (2016). In M. Svoboda, & B. A. Fuchs (Eds.), *Handbook of drought indicators and indices, Integrated Drought Management Tools and Guidelines Series 2*, (). Geneva: Integrated Drought Management Programme (IDMP).

Xu, X. L., Liu, W., Scanlon, B. R., Zhang, L., & Pan, M. (2013). Local and global factors controlling water-energy balances within the Budyko framework. *Geophysical Research Letters*, *40*, 6123–6129. https://doi.org/10.1002/2013GL058324

Yan, H., Wang, S. Q., Lu, H. Q., Yu, Q., Zhu, Z. C., Myneni, R. B., et al. (2014). Development of a remotely sensing seasonal vegetation-based Palmer drought severity index and its application of global drought monitoring over 1982–2011. *Journal of Geophysical Research: Atmospheres*, *119*, 9419–9440. https://doi.org/10.1002/2014JD021673

Yan, H., Wang, S. Q., Wang, J. B., Lu, H. Q., Guo, A. H., Zhu, Z. C., et al. (2016). Assessing spatiotemporal variation of drought in China and its impact on agriculture during 1982–2011 by using PDSI indices and agriculture drought survey data. *Journal of Geophysical Research: Atmospheres*, *121*, 2283–2298. https://doi.org/10.1002/2015JD024285

Yang, D. W., Sun, F. B., Liu, Z. Y., Cong, Z. T., & Lei, Z. D. (2006). Interpreting the complementary relationship in non-humid environments based on the Budyko and penman hypotheses. *Geophysical Research Letters*, *33*, L18402. https://doi.org/10.1029/2006GL027657

Yang, D. W., Sun, F. B., Liu, Z. Y., Cong, Z. T., Ni, G. H., & Lei, Z. D. (2007). Analyzing spatial and temporal variability of annual water-energy balance in non-humid regions of China using the Budyko hypothesis. *Water Resources Research*, *43*, W04426. https://doi.org/10.1029/2006WR005224

Yang, Y. T., Roderick, M. L., Zhang, S. L., McVicar, T. R., & Donohue, R. J. (2018). Hydrologic implications of vegetation response to elevated CO2 in climate projections. *Nature Climate Change*, *9*(1), 44–48. https://doi.org/10.1038/s41558-018-0361-0

Yang, Y. T., Zhang, S. L., McVicar, T. R., Beck, H. E., Zhang, Y. Q., & Liu, B. (2018). Disconnection between trends of atmospheric drying and continental runoff. *Water Resources Research*, *54*, 4700–4713. https://doi.org/10.1029/2018WR022593

Yin, D. Q., Roderick, M. L., Leech, G., Sun, F. B., & Huang, Y. F. (2014). The contribution of reduction in evaporative cooling to higher surface air temperatures during drought. *Geophysical Research Letters*, *41*, 7891–7897. https://doi.org/10.1002/2014GL062039

Zhang, B. Q., AghaKouchak, A., Yang, Y., Wei, J., & Wang, G. (2019). A water-energy balance approach for multi-category drought assessment across globally diverse hydrological basins. *Agricultural and Forest Meteorology*, *264*, 247–265. https://doi.org/10.1016/j.agrformet.2018.10.010

Zhang, B. Q., Wang, Z. K., & Chen, G. (2017). A sensitivity study of applying a two-source potential evapotranspiration model in the standardized precipitation evapotranspiration index for drought monitoring. *Land Degradation & Development*, *28*, 783–793. https://doi.org/10.1002/ldr.2548

Zhang, B. Q., Wu, P. T., Zhao, X. N., & Gao, X. D. (2014). Spatiotemporal analysis of climate variability (1971–2010) in spring and summer on the loess plateau, China. *Hydrological Processes*, *28*, 1689–1702. https://doi.org/10.1002/hyp.9724

Zhang, B. Q., Zhao, X. N., Jin, J. M., & Wu, P. T. (2015). Development and evaluation of a physically based multiscalar drought index: The standardized moisture anomaly index. *Journal of Geophysical Research: Atmospheres*, *120*, 11,575–11,588. https://doi.org/10.1002/2015JD023772